Improved Model Predictive Current Control for SPMSM Drives Using Current Update Mechanism

Xin Yuan, *Student Member IEEE*, Shuo Zhang, *Member IEEE*, Chengning Zhang, Alessandro Galassini, *Member IEEE*, Giampaolo Buticchi, *Senior Member IEEE*, Michele Degano, *Member IEEE*

***Abstract*—Finite-Set Model Predictive Current Control (FS-MPCC) has been employed for machine drives owing to the good dynamic performance. Sensitivity to parameter variation is one of the main barriers to its widespread application. To overcome this barrier, this work proposes an improved FS-MPCC for Surfaced Permanent Magnet Synchronous Machines (SPMSMs). The contribution of this work is developing a novel current update mechanism, where the variation of resistance, rotor flux linkage and inductance is considered, in which a modified coordinate system which contains a stationary and rotary axis frame is introduced. In this case, the predicted parameter can be obtained more accurately based on this mechanism, which can suppress the disturbances caused by model parameter mismatch. In addition, SPMSM parameter mismatch effect on FS-MPCC performance is analyzed in this paper, which testifies that resistance mismatch influence on current prediction error can be neglected in practical system. The proposed FS-MPCC is validated and compared against different state-of-the-art methods. Improvement of the proposed control strategy is validated by means of experimental results on a 2-kW test rig.**

***Index Terms*—Surfaced permanent magnet synchronous machines (SPMSMs), finite-set model predictive current control (FS-MPCC), model parameter mismatch.**

NOMENCLATURE

ω_m, ω_e	Mechanical and electrical angular speed
p	The number of pole pairs
R	Motor stator resistance
L	Motor stator inductance
Ψ_m	Motor rotor flux linkage
T_e, T_l	Electromagnetic torque and load torque
θ, θ_r	Electrical angle and rotor position
η, B	Inertia and viscous friction coefficient.
T_s	Sampling period
U_s^{opt}	Optimum voltage vector
$\overline{R}$	Initial motor stator resistance
$\overline{L}$	Initial motor stator inductance
$\overline{\Psi_m}$	Initial motor rotor flux linkage

Manuscript received Sep. 15, 2019; revised Nov. 19, 2019, and Jan. 9, 2020; accepted Feb. 4, 2020. This work was supported by Research and development plan in key areas of guangdong province under Grant NO.2019B090910001.

Xin Yuan, Shuo Zhang and Chengning Zhang are with the School of Mechanical Engineering and Collaborative Innovation Center of Electric Vehicles in Beijing, Beijing Institute of Technology, Beijing, 100081, China(email:yuanxinedu@gmail.com;shuozhangxd@163.com;chengningzhangIEEE@163.com)

Michele Degano and Alessandro Galassini are with PEMC group, University of Nottingham, U.K. (email:Michele.degano@nottingham.ac.uk;alessandro.galassini@nottingham.ac.uk)

Giampaolo Buticchi is with PEMC group, University of Nottingham Ningbo China, China, email: giampaolo.buticchi@nottingham.edu.cn.

I. INTRODUCTION

SPMSMs [1]-[2] are widely used in industrial application owing to high power density and high efficiency. In terms of motor control strategies, conventional linear Proportional-Integral control is extensively employed in SPMSM drives [3], but the transient performance is not optimum. In this case, it is necessary to develop novel motor control strategies in SPMSMs drives. In recent years, due to simple implementation, faster dynamic response and straightforward handling of nonlinearities and constraints, Model Predictive Control (MPC) has gotten extensive attention [4]. The principle is to predict the future behavior of the variables within several sampling time on the basic of cost function, and then, the sequence that minimizes the cost function is chosen. Although the MPC has been implemented in some motor drives and power converter applications, if compared to conventional control strategies, the required calculation is higher [5]. To simplify the prediction calculation of the system behavior, finite-set model predictive control (FS-MPC) was proposed [6]. Taking advantage of the discrete nature of voltage source inverters, there are only few number of possible switching states. In order to reduce the torque ripple, FS-MPC with optimal duty cycle was proposed by inserting a zero vector with the selected voltage vector [7]. The zero vector duration is determined based on the duty cycle control principle. Since conventional FS-MPC suffers from weighting factor tuning work, authors in [8] proposed an improved FS-MPC without weighting factor to control torque and flux in induction machine drives. To further decrease the computational burden in low cost microprocessors, authors in [9] proposed an improved FS-MPC with one-step prediction to obtain the optimum voltage vector.

However, FS-MPC strongly depends on system models, and model parameter disturbances can occur often with different operating conditions, which can deteriorate FS-MPC performance. For instant, a 20 % rotor flux linkage reduction occurs with ambient temperature increases by 100 ℃ [10]. If a fixed rotor flux linkage is set in the control system the prediction current errors would be amplified. Since the approach of offline machine parameter identification is time-consuming, few online approaches to predict rotor flux linkage were proposed before. Authors in [11] developed a Kalman filter and a Luenberger observer to obtain the rotor position, which can suppress the model disturbances. Authors in [12] presented an adaptive sliding mode observer to obtain the value of third harmonic rotor flux linkage, which can suppress the third rotor order flux linkage disturbances. To suppress the external disturbances such as friction torque, load torque and mechanical factors, authors in [13] proposed an improved sliding mode observer with a novel sliding mode reaching law in PMSM system. Since the flux linkage and inductance disturbances can amplify torque ripple, an incremental model for PMSM is introduced in [14]. Herein, it can be found that the rotor flux linkage disturbances are fundamentally eliminated in the novel machine model of [14]. Authors in [15] proposed an improved flux observer with fuzzy algorithm to eliminate flux linkage disturbances. In order to observe the actual inductance, authors in [16] proposed an extended state observer with PMSM incremental model. In [17], a disturbance rejection control (ADRC) based on Proportional-Integral-Derivative controller is introduced. ADRC was used in induction motors to predict and compensate the disturbances caused by parameters mismatch [18]. In order to suppress periodic disturbances, iterative learning control (ILC) is employed. Authors in [19] proposed a robust ILC to suppress the disturbances caused by current offsets and scaling errors in PMSM drives. Because thermal drift can increase the offset voltage variation of current sensors, a novel current offset error compensator is designed to suppress this disturbance [20]. Authors in [21] proposed internal model control in speed loop to suppress the external disturbances caused by the inertia of PMSM. To testify the theoretical robustness of FS-MPC, the stability with a control-Lyapunov function was introduced in [22]. In order to suppress the disturbances caused by PMSM inductance and flux linkage parameters mismatch, an improved MPC based on a current error correction with high frequency suppression was proposed [23]. In addition, authors in [23] proved the current error to be caused mainly by the mismatch of both flux linkage and inductance parameters. Authors in [24] proposed a robust predictive current control based on a discrete-time integral term to suppress the disturbances caused by the PMSM parameter mismatch. However, [23] and [24] are only applied in dead-beat MPC. Authors in [25] analyzed the effect of model parameter uncertainties on the current prediction error of FS-MPC, but it is only applied in three-phase inverter application.

Recently, an improved FS-MPC without utilizing machine model parameters has been proposed. This method predicts the next instant current based on measured currents [26]-[27]. To suppress inductance mismatch disturbances, a modified FS-MPC with prediction error correction was proposed in [28]-[29]. However, the slow current update would occur when the current instant switching state is the same with the previous instant switching state, which can deteriorate the current performance. In order to avoid the slow current update, authors in [30] proposed a modified FS-model predictive current control (FS-MPCC) with a current variation update mechanism. The principle is to utilize previous instant measured currents and predicted currents to obtain new SPMSM model parameters. However, this modified FS-MPCC only aimed at the SPMSM under the assumption that the electrical angle at the adjacent instant can be approximately equal, which can affect the estimated parameter accuracy and the current performance.

The contribution of this work is that this paper proposes an improved FS-MPCC with the state-of-the-art current update mechanism to suppress the disturbances. Although, [30] has developed a modified FS-MPCC to overcome this problem, [30] assumed that the adjacent instant machine electrical angle is the same. In this case, the error can affect the estimated parameter accuracy of the modified FS-MPCC. Especially in high-speed region, the value of the estimated parameter disturbances can be further amplified. To overcome this problem, a novel current update mechanism which contains a stationary and rotary axis frame is proposed. In the novel current update mechanism, estimated parameters can be obtained more accurate than that in [30] and can be applied in high-speed SPMSM applications. These obtained parameters can suppress the disturbances caused by parameters mismatch and enhance system robustness. In addition, SPMSM parameter mismatch effect on FS-MPCC performance has been analyzed in detail. Finally, the proposed method is compared against conventional FS-MPCC and FS-MPCC in [30] through a 2-kW test rig.

This paper is organized as follows: the conventional FS-MPCC and SPMSM mathematical model are introduced in Section II. The specific procedure of the proposed method and the parameter disturbances effect on FS-MPCC performance are introduced in Section III. Experiment is carried out in Section IV. Finally, the conclusions are derived in Section V.

II. Conventional Finite-Set Model Predicative Current Control

In this section, the SPMSM mathematical model and conventional FS-MPCC are briefly introduced.

A. SPMSM Mathematical Model

In this paper, the following assumptions regarding the SPMSM mathematical model [31] have been made, which are noted as follows. Magnetic saturation, cogging torque and cross-saturation [32] are not considered in this paper. Therefore, it means that the inductance on d axis is approximately equal to the inductance on q axis and equal to the inductance on stationary alpha and beta axis, namely $L_d = L_q = L_s = L$. The mathematical model of SPMSM on dq axis can be presented as follows.

$$\begin{cases} U_d = Ri_d + L\dfrac{di_d}{dt} - \omega_e L i_q \\ U_q = Ri_q + L\dfrac{di_q}{dt} + \omega_e L i_d + \omega_e \psi_m \end{cases} \tag{1}$$

$$T_e=1.5p\psi_m i_q \tag{2}$$

$$T_e\text{-}T_l=\eta\frac{d\omega_m}{dt}+B\omega_m \tag{3}$$

where i_d and i_q stand for the stator currents on dq axis, respectively; U_d and U_q stand for the stator voltages on dq axis, respectively.

B. Conventional FS-MPCC

To obtain the next instant currents on dq axis, the first-order forward Euler discretization is employed. The SPMSM current model is presented in Eq. (4).

$$\begin{cases} i_d(k+1)=i_d(k)-\dfrac{T_sR}{L}i_d(k)+T_s\omega_e(k)i_q(k)+\dfrac{T_s}{L}U_d(k) \\ i_q(k+1)=i_q(k)-\dfrac{T_sR}{L}i_q(k)-T_s\omega_e(k)i_d(k)-\dfrac{T_s\psi_{\mathrm{m}}}{L}\omega_{\mathrm{e}}(k) \\ \qquad\qquad +\dfrac{T_s}{L}U_q(k) \end{cases} \tag{4}$$

In the FS-MPCC of a two-level inverter, there are only eight switching states namely U_0, U_1, U_2, U_3, U_4, U_5, U_6, U_7, which are presented in Table I. U_{dc} denotes the value of dc bus voltage in the system.

TABLE I
SWITCHING STATE OF SPMSM

Switching state	U_s	U_α	U_β
U_0	0	0	0
U_1	$\frac{2U_{dc}}{3}$	$\frac{2U_{dc}}{3}$	0
U_2	$\frac{U_{dc}}{3}+\frac{U_{dc}}{3}*j$	$\frac{U_{dc}}{3}$	$\frac{U_{dc}}{\sqrt{3}}$
U_3	$\frac{-U_{dc}}{3}+\frac{U_{dc}}{3}*j$	$\frac{-U_{dc}}{3}$	$\frac{U_{dc}}{\sqrt{3}}$
U_4	$\frac{-2U_{dc}}{3}$	$\frac{-2U_{dc}}{3}$	0
U_5	$\frac{-U_{dc}}{3}-\frac{U_{dc}}{3}*j$	$-\frac{U_{dc}}{3}$	$-\frac{U_{dc}}{\sqrt{3}}$
U_6	$\frac{U_{dc}}{3}-\frac{U_{dc}}{3}*j$	$\frac{U_{dc}}{3}$	$-\frac{U_{dc}}{\sqrt{3}}$
U_7	0	0	0

Since there is one-step delay in the practical system, the delay compensation method in [33] is employed in this paper. The (k+2)th predicted currents can be expressed in Eq. (5), where the subscript $sw=i$ ($i=0,1,2\ldots,6,7$) denotes the switching state of the inverter. Owing to the characteristic of the two-level inverter topology, the subscript sw can have 8 types of switching states. Because the mechanical time constant of SPMSM is much larger than the electromagnetic time constant, the motor rotor speed can be considered as constant during two control periods, namely $\omega_e(k)\approx\omega_e(k+1)$. In addition, according to the first-order forward Euler discretization, the next instant θ can be simply obtained as follows.

$$\theta(k+1)=\theta(k)+\omega_e(k)T_{\mathrm{s}} \tag{6}$$

To satisfy the minimum current errors between the command and prediction, cost function is designed in Eq. (7). Finally, the optimum voltage vector is obtained by minimizing the cost function J_{min}.

$$J_{\min}=\left|i_d^{\ ref}(k+2)-i_d(k+2)\right|+\left|i_q^{\ ref}(k+2)-i_q(k+2)\right| \tag{7}$$

Therefore, U_s^{opt} can be obtained according to Eq. (7). The diagram of the conventional FS-MPCC in SPMSM drives is shown in Fig. 1.

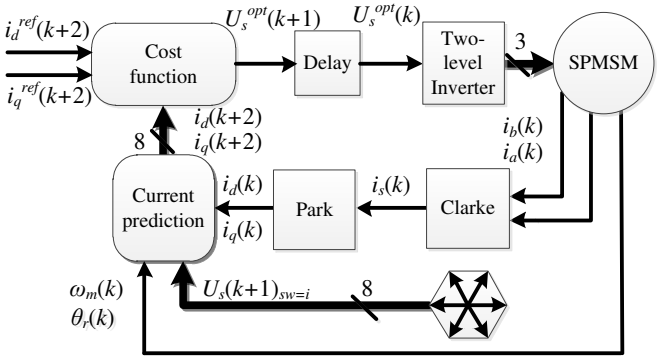

Fig. 1. FS-MPCC diagram in SPMSM drives.

III. IMPROVED MODEL PREDICTIVE CURRENT CONTROL WITH PARAMETER MISMATCH SUPPRESSION

The effect of SPMSM model parameters on FS-MPCC is analyzed in Section A. From the analysis, it can be found that the parameter disturbances can deteriorate the FS-MPCC current performance much. Thus, an improved FS-MPCC with the state-of-the-art current update mechanism is introduced in Section B.

A. Parameter mismatch effect on FS-MPCC performance

In practical applications, the value of SPMSM parameters cannot be fixed with different operating conditions. The SPMSM current prediction model under parameter mismatch can be presented as follows.

$$\begin{cases} \overline{i_d}(k+1)=i_d(k)-\dfrac{T_s\overline{R}}{\overline{L}}i_d(k)+T_s\omega_e(k)i_q(k)+\dfrac{T_s}{\overline{L}}U_d(k) \\ \overline{i_q}(k+1)=i_q(k)-\dfrac{T_s\overline{R}}{\overline{L}}i_q(k)-T_s\omega_e(k)i_d(k)-\dfrac{T_s\overline{\psi_{\mathrm{m}}}}{\overline{L}}\omega_{\mathrm{e}}(k) \\ \qquad\qquad +\dfrac{T_s}{\overline{L}}U_q(k) \end{cases} \tag{8}$$

where $\overline{i_d}$ (k+1) and $\overline{i_q}$ (k+1) denote the (k+1)th instant predicted currents. If the (k+1) instant predicted current is inaccurate, U_s^{opt} might be not optimum according to Eq. (5) and Eq. (7). In this case, the FS-MPCC performance would be decreased owing to a sub-optimal voltage vector selection. According to Eq. (4) and Eq. (8), the current errors between the models with and without parameter mismatch are presented as follows.

$$\begin{cases} e_d(k)=\left(\dfrac{\overline{R}}{\overline{L}}-\dfrac{R}{L}\right)T_si_d(k)+\left(\dfrac{1}{L}-\dfrac{1}{\overline{L}}\right)T_sU_d(k) \\ e_q(k)=\left(\dfrac{\overline{R}}{\overline{L}}-\dfrac{R}{L}\right)T_si_q(k)+\left(\dfrac{\overline{\psi_{\mathrm{m}}}}{\overline{L}}-\dfrac{\psi_{\mathrm{m}}}{L}\right)T_s\omega_{\mathrm{e}}(k)+\left(\dfrac{1}{L}-\dfrac{1}{\overline{L}}\right)T_sU_q(k) \end{cases} \tag{9}$$

where $e_d(k)$ and $e_q(k)$ denote the current error. From Eq. (9), it can be seen that resistance, inductance and flux linkage mismatches all affect the current error. The relationship between $e_d(k)$ and $e_q(k)$ is shown in Figs. 2–3. From the

$$\begin{cases} i_d(k+1)=i_d(k)-\dfrac{T_sR}{L}i_d(k)+T_s\omega_e(k)i_q(k)+\dfrac{T_s}{L}\left[U_\alpha(k)\cos\left(\theta(k)\right)+U_\beta(k)_{sw=i}\sin\left(\theta(k)\right)\right] \\ i_d(k+2)=i_d(k+1)-\dfrac{T_sR}{L}i_d(k+1)+T_s\omega_e(k+1)i_q(k+1)+\dfrac{T_s}{L}\left[U_\alpha(k+1)_{sw=i}\cos\left(\theta(k+1)\right)+U_\beta(k+1)_{sw=i}\sin\left(\theta(k+1)\right)\right] \\ i_q(k+1)=i_q(k)-\dfrac{T_sR}{L}i_q(k)-T_s\omega_e(k)i_d(k)-\dfrac{T_s\psi_{\mathrm{m}}}{L}\omega_{\mathrm{e}}(k)+\dfrac{T_s}{L}\left[-U_\alpha(k)\sin\left(\theta(k)\right)+U_\beta(k)_{sw=i}\cos\left(\theta(k)\right)\right] \\ i_q(k+2)=i_q(k+1)-\dfrac{T_sR}{L}i_q(k+1)-T_s\omega_e(k+1)i_d(k+1)-\dfrac{T_s\psi_{\mathrm{m}}}{L}\omega_{\mathrm{e}}(k+1)+\dfrac{T_s}{L}\left[-U_\alpha(k+1)_{sw=i}\sin\left(\theta(k+1)\right)+U_\beta(k+1)_{sw=i}\cos\left(\theta(k+1)\right)\right] \end{cases} \tag{5}$$

simulation results, it can be seen that the resistance value is quite small and cannot affects the current error much. At 100 r/min condition, the inductance mismatch can affect the current error dramatically. Whereas, at 1200 r/min condition, inductance mismatch and flux linkage mismatch can much affect the current error together. The effect of flux linkage mismatch on current error becomes obvious with the SPMSM speed rising. In addition, it can be seen that the inductance mismatch mainly can affect the current error fluctuation. Flux linkage and resistance mismatches mainly affect the current error offset. Therefore, it is meaningful to suppress the model parameter mismatch disturbances, especially in inductance and flux linkage mismatch disturbances. To suppress the model parameter mismatch disturbances, it is inevitable to develop an improved FS-MPCC.

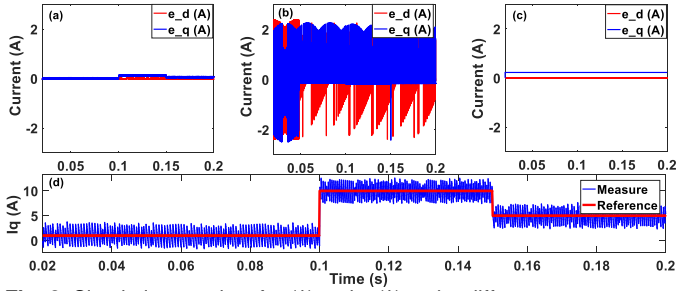

Fig. 2. Simulation results of $e_d(k)$ and $e_q(k)$ under different parameter mismatch at 100 r/min. (a) $\bar{R}=2R$. (b) $\bar{L}=2L$. (c) $\overline{\Psi_{\mathrm{m}}}=2\Psi_{\mathrm{m}}$. (d) the current on q axis

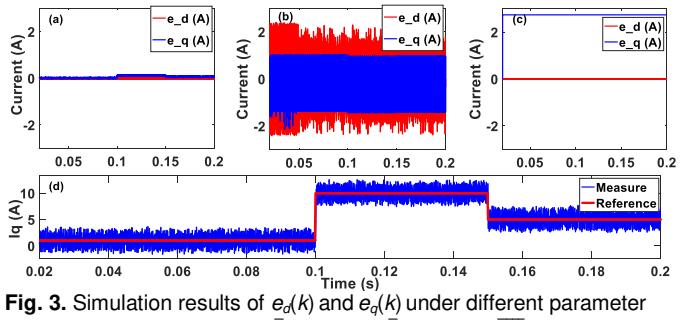

Fig. 3. Simulation results of $e_d(k)$ and $e_q(k)$ under different parameter mismatch at 1200 r/min. (a) $\bar{R}=2R$. (b) $\bar{L}=2L$. (c) $\overline{\Psi_{\mathrm{m}}}=2\Psi_{\mathrm{m}}$. (d) the current on q axis

B. The state-of-the-art FS-MPCC with current variation update mechanism

The previous method in [30] utilized a current variation mechanism to suppress the disturbances caused by parameter mismatch effectively. This can be expressed as in Eqs. (10-13). According to the following equations, the SPMSM inductance value can be predicted.

$$\overline{i_\alpha}(k)\text{-}i_\alpha(k)=\left(\frac{T_s}{\bar{L}}-\frac{T_s}{L}\right)U_\alpha(k\text{-}1)-\overbrace{\left[\bar{R}\frac{T_s}{\bar{L}}-R\frac{T_s}{L}\right]i_\alpha(k\text{-}1)}^{Term\,1} \\ +\overbrace{\left(\overline{\psi_m}\frac{T_s}{\bar{L}}-\psi_m\frac{T_s}{L}\right)\omega_e(k\text{-}1)\sin\left(\theta(k\text{-}1)\right)}^{Term\,2} \tag{10}$$

$$\overline{i_\beta}(k)\text{-}i_\beta(k)=\left(\frac{T_s}{\bar{L}}-\frac{T_s}{L}\right)U_\beta(k\text{-}1)-\overbrace{\left[\bar{R}\frac{T_s}{\bar{L}}-R\frac{T_s}{L}\right]i_\beta(k\text{-}1)}^{Term\,3} \\ -\overbrace{\left(\overline{\psi_m}\frac{T_s}{\bar{L}}-\psi_m\frac{T_s}{L}\right)\omega_e(k\text{-}1)\cos\left(\theta(k\text{-}1)\right)}^{Term\,4} \tag{11}$$

$$\Delta\sigma_\alpha(k)=\left[\overline{i_\alpha}(k)\text{-}i_\alpha(k)\right]-\left[\overline{i_\alpha}(k\text{-}1)\text{-}i_\alpha(k\text{-}1)\right] \\ \approx\left(\frac{T_s}{\bar{L}}-\frac{T_s}{L}\right)\left[U_\alpha(k\text{-}1)-U_\alpha(k\text{-}2)\right] \tag{12}$$

$$\Delta\sigma_\beta(k)=\left[\overline{i_\beta}(k)\text{-}i_\beta(k)\right]-\left[\overline{i_\beta}(k\text{-}1)\text{-}i_\beta(k\text{-}1)\right] \\ \approx\left(\frac{T_s}{\bar{L}}-\frac{T_s}{L}\right)\left[U_\beta(k\text{-}1)-U_\beta(k\text{-}2)\right] \tag{13}$$

where $i_\alpha(k)$ and $i_\beta(k)$ denote the measured current on the stationary alpha and beta axis at the kth instant; $\overline{i_\alpha}(k)$ and $\overline{i_\beta}(k)$ denote the kth instant predicted current. $U_\alpha(k\text{-}1)$ and $U_\beta(k\text{-}1)$ denote the measured motor voltage on the stationary alpha and beta axis at the $(k\text{-}1)$th instant. $\Delta\sigma_\alpha(k)$ and $\Delta\sigma_\beta(k)$ denote the contiguous instant current variation between the predicted and measured currents at the kth instant. In this method, it is assumed that the impact of the resistive voltage drop $Ri_\alpha(k\text{-}1)$ and $Ri_\beta(k\text{-}1)$ can be neglected if the last instant voltage vector is not a zero vector [28]-[30]. The reason is because there are only eight switching states in FS-MPCC, the amplitude of SPMSM stator voltage is much larger than the amplitude of the resistive voltage drop, namely $|Ri_\alpha(k\text{-}1)| << |U_\alpha(k\text{-}1)|$ and $|Ri_\beta(k\text{-}1)| << |U_\beta(k\text{-}1)|$. In this case, the value of *Term* 1 and *Term* 3 at the adjacent control period is equal to zero.

However, when the SPMSM model parameters mismatch with the real SPMSM parameters, it is also assumed that the variation of SPMSM electrical angle at the adjacent control period is approximately equal to zero [30], which means that the variation of the *Term* 2 and *Term* 4 at the adjacent control period is equal to zero, which is presented in Eq. (14).

$$\begin{cases} \Delta Term\,2 = \left(\psi_m \dfrac{T_s}{L} - \psi_m \dfrac{T_s}{L}\right) \overbrace{\begin{bmatrix} \omega_e(k-1)\sin\left(\theta(k-1)\right) \\ -\omega_e(k-2)\sin\left(\theta(k-2)\right) \end{bmatrix}}^{Z_\alpha} \approx 0 \\ \Delta Term\,4 = \left(\psi_m \dfrac{T_s}{L} - \psi_m \dfrac{T_s}{L}\right) \overbrace{\begin{bmatrix} \omega_e(k-1)\cos\left(\theta(k-1)\right) \\ -\omega_e(k-1)\cos\left(\theta(k-1)\right) \end{bmatrix}}^{Z_\beta} \approx 0 \end{cases} \tag{14}$$

To analyze the influence on the current performance, Z_α and Z_β is defined as the variation of the *Term* 2 and *Term* 4 at the adjacent instant in Eq. (14). Fig. 4 shows that the amplitude of Z_α and Z_β under different speed conditions. It can be seen that the value of Z_α and Z_β increases with the speed rising. Thus, the above assumption cannot be neglected otherwise the control performance can be affected in negative way. Especially, in high-speed SPMSM, the value of the variation of Z_α and Z_β at the adjacent instant becomes large.

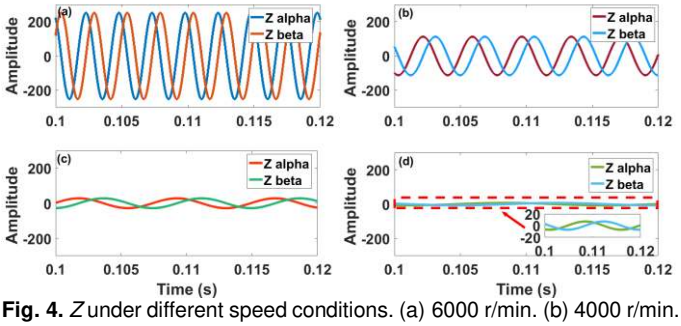

Fig. 4. *Z* under different speed conditions. (a) 6000 r/min. (b) 4000 r/min. (c) 2000 r/min. (d) 1000 r/min.

To suppress the disturbances caused by the variation of SPMSM electrical angle in [30], an improved FS-MPCC with novel current update mechanism is proposed in this paper. The specific procedure is presented as follows. First, the last instant measured motor current $i_s(k\text{-}1)$ and voltage $U_s(k\text{-}1)$ are stored in the microprocessor. On the stationary alpha and beta axis, the equations can be presented as follows.

$$i_\alpha(k) - i_\alpha(k-1) = \frac{T_s}{L}\begin{bmatrix} U_\alpha(k-1) - Ri_\alpha(k-1) \\ +\psi_m\omega_e(k-1)\sin\left(\theta(k-1)\right) \end{bmatrix} \tag{15}$$

$$i_\beta(k) - i_\beta(k-1) = \frac{T_s}{L}\begin{bmatrix} U_\beta(k-1) - Ri_\beta(k-1) \\ -\psi_m\omega_e(k-1)\cos\left(\theta(k-1)\right) \end{bmatrix} \tag{16}$$

According to Eq. (16), the term of flux linkage can be presented as follows.

$$-\frac{T_s}{L}\psi_m\omega_e(k-1) = \frac{i_\beta(k) - i_\beta(k-1) - \dfrac{T_s}{L}U_\beta(k-1) + \dfrac{T_s}{L}Ri_\beta(k-1)}{\cos\left(\theta(k-1)\right)} \tag{17}$$

Substituting Eq. (17) into Eq. (15), Eq. (18) can be presented as follows.

$$\begin{aligned} &\frac{T_s}{L}\begin{bmatrix} U_\alpha(k-1)\cos\left(\theta(k-1)\right) + U_\beta(k-1)\sin\left(\theta(k-1)\right) \\ -R\left(i_\alpha(k-1)\cos\left(\theta(k-1)\right) + i_\beta(k-1)\sin\left(\theta(k-1)\right)\right) \end{bmatrix} \\ &= \left(i_\beta(k) - i_\beta(k-1)\right)\sin\left(\theta(k-1)\right) + \left(i_\alpha(k) - i_\alpha(k-1)\right)\cos\left(\theta(k-1)\right) \end{aligned} \tag{18}$$

Since the impact of the resistive voltage drop $Ri_\alpha(k\text{-}1)$ and $Ri_\beta(k\text{-}1)$ can be neglected, the equation can be satisfied as follows.

$$\begin{aligned} &U_\alpha(k-1)\cos\left(\theta(k-1)\right) + U_\beta(k-1)\sin\left(\theta(k-1)\right) \approx \\ &\cos\left(\theta(k-1)\right)\left[U_\alpha(k-1) - Ri_\alpha(k-1)\right] \\ &+\sin\left(\theta(k-1)\right)\left[U_\beta(k-1) - Ri_\beta(k-1)\right] \end{aligned} \tag{19}$$

Afterwards, define K as $\frac{T_s}{L}$, Eq. (18) can be rearranged into Eq. (20).

$$K = \frac{T_s}{L} = \frac{\begin{Bmatrix} \left[i_\alpha(k) - i_\alpha(k-1)\right]\cos\left(\theta(k-1)\right) \\ +\left[i_\beta(k) - i_\beta(k-1)\right]\sin\left(\theta(k-1)\right) \end{Bmatrix}}{\begin{bmatrix} U_\alpha(k-1)\cos\left(\theta(k-1)\right) \\ +U_\beta(k-1)\sin\left(\theta(k-1)\right) \end{bmatrix}} \tag{20}$$

When the denominator in Eq. (20) is approximately equal to zero, K cannot be obtained accurately. In this case, assuming Eq. (21) needs to be satisfied in the proposed method, parameter K can be updated and stored in the FS-MPCC. When the denominator in Eq. (20) does not satisfy Eq. (21), the latest obtained parameter K will be utilized until the new obtained parameter K is acquired through Eq. (20). X requires a tuning phase. The diagram of parameter K acquisition is presented in Fig. 5.

$$\left|U_\alpha(k-1)\cos\left(\theta(k-1)\right) + U_\beta(k-1)\sin\left(\theta(k-1)\right)\right| > X \tag{21}$$

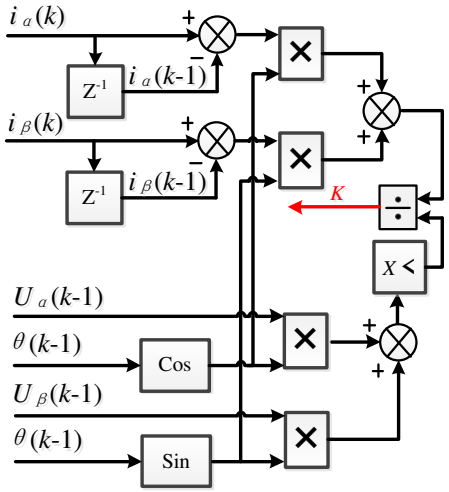

Fig. 5. The diagram of parameter *K* acquisition

After acquiring K, the current equation on dq axis based on Eq. (4) needs to be built to avoid the variation of θ instead of using the current equation on stationary alpha and beta axis. Eq. (4) at the $(k\text{-}1)$th instant can be rearranged as follows.

$$\begin{cases} -\dfrac{T_sR}{L}i_d(k-1) + T_s\omega_e(k-1)i_q(k-1) \\ \qquad = i_d(k) - i_d(k-1) - KU_d(k-1) \\ -\dfrac{T_sR}{L}i_q(k-1) - T_s\omega_e(k-1)i_d(k-1) - \dfrac{T_s\psi_m}{L}\omega_e(k-1) \\ \qquad = i_q(k) - i_q(k-1) - KU_q(k-1) \end{cases} \tag{22}$$

In Eq. (22) on d axis, since SPMSM is adopted in this paper, $i_d(k\text{-}1) \approx i_d(k)$, Eq. (22) on d axis can be rearranged as follows.

$$-\frac{T_sR}{L}i_d(k) = i_d(k) - i_d(k-1) - KU_d(k-1) - T_s\omega_e(k-1)i_q(k-1)$$

(23)

$\frac{T_s R}{L}$ can be obtained based on Eq. (23) and is substituted into Eq. (22) on q axis, which can be expressed as.

$$-\frac{T_s\psi_m}{L}\omega_e(k-1)=i_q(k)-i_q(k-1)+\frac{T_sR}{L}i_q(k-1) \\ -KU_q(k-1)+T_s\omega_e(k-1)i_d(k-1) \tag{24}$$

Since $\omega_e(k\text{-}1)\approx\omega_e(k)$, Eq. (24) can be rearranged in Eq. (25).

$$-\frac{T_s\psi_m}{L}\omega_e(k)=i_q(k)-i_q(k-1)+\frac{T_sR}{L}i_q(k-1) \\ -KU_q(k-1)+T_s\omega_e(k-1)i_d(k-1) \tag{25}$$

Without considering one-step delay compensation, the specific acquisition of $i_d(k+1)$ and $i_q(k+1)$ can be expressed in Fig. 6.

If considering one-step delay compensation, according to Eq. (4), Eq. (23) and Eq. (25), the $i_d(k+1)$ and $i_q(k+1)$ can be acquired in Eq. (26).

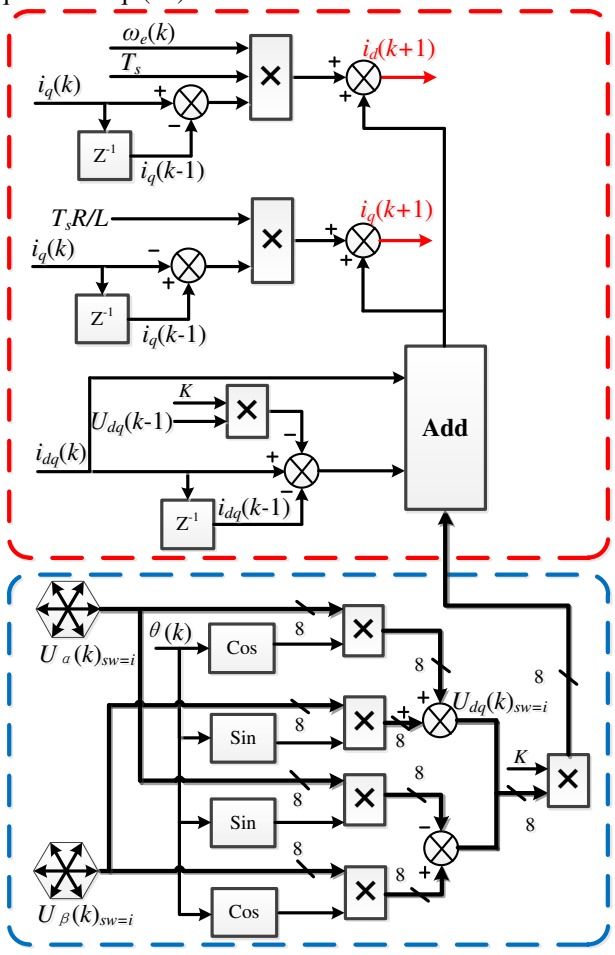

Fig. 6. The diagram of $i_d(k+1)$ and $i_q(k+1)$ acquisition.

$$\begin{cases} i_d(k+1)=2i_d(k)-i_d(k-1)+K\left[U_d(k)-U_d(k-1)\right] \\ \quad +T_s\omega_e(k)\left[i_q(k)-i_q(k-1)\right] \\ i_q(k+1)=2i_q(k)-i_q(k-1)+K\left[U_q(k)-U_q(k-1)\right] \\ \quad -\frac{T_sR}{L}\left[i_q(k)-i_q(k-1)\right] \end{cases} \tag{26}$$

After obtaining the $(k+1)$ instant predicted currents, the $(k+2)$ instant predicted currents can be obtained in Eq. (27) based on Eq. (5). The optimum voltage can be selected according to the principle of the cost function minimization. The proposed MPCC diagram is shown in Fig. 7.

$$\begin{cases} i_d(k+2)=i_d(k+1)-\frac{T_sR}{L}i_d(k+1)+T_s\omega_e(k)i_q(k+1) \\ \quad +KU_d(k+1)_{sw=i} \\ i_q(k+2)=i_q(k+1)+i_q(k)+\frac{T_sR}{L}\left[i_q(k-1)-i_q(k+1)\right] \\ \quad +K\left(U_q(k+1)_{sw=i}-U_q(k-1)\right)-i_q(k-1) \\ U_d(k+1)_{sw=i}=\begin{bmatrix} U_\alpha(k+1)_{sw=i}\cos\left(\theta(k+1)\right) \\ +U_\beta(k+1)_{sw=i}\sin\left(\theta(k+1)\right)\end{bmatrix} \\ U_q(k+1)_{sw=i}=\begin{bmatrix} -U_\alpha(k+1)_{sw=i}\sin\left(\theta(k+1)\right) \\ +U_\beta(k+1)_{sw=i}\cos\left(\theta(k+1)\right)\end{bmatrix} \end{cases} \tag{27}$$

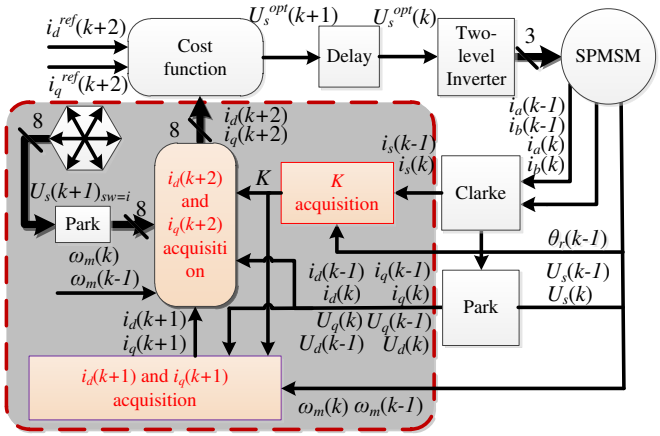

Fig. 7. Proposed MPCC diagram for SPMSM drives.

IV. Experimental Results

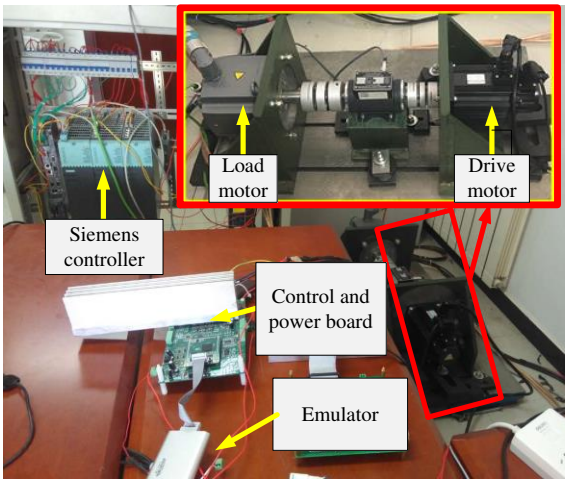

Fig. 8. Diagram of the test rig for SPMSM drives.

TABLE II
SPMSM Parameters

Parameter	Description	Value
P_N (kW)	Rated power	2
p	Number of pole pairs	4
R (Ω)	Stator resistance	0.365
L (mH)	Stator inductance	1.225
Ψ_m (Wb)	Rotor flux linkage	0.1667
T_N (Nm)	Rated torque	10
I_N (A)	Rated Current	10

n_N(krpm)	Rated Speed	2

To verify the effectiveness of the proposed control method the test rig is constructed as displayed in Fig. 8. The load motor and motor controller are produced by Siemens Company. The rated power of load motor is 5.6-kW and the rated power of drive motor is 2-kW. The main parameters of the drive motor are displayed in Table II. The control system for the drive motor includes a type of XDS200ISO emulator, DSP control board (the control chip is TMS320F28377d), power board, PC, and power supply. The system sampling period T_s is 33 us. Three methods are compared in this paper, namely a conventional FS-MPCC (Method 1), an improved FS-MPCC in [30] (Method 2) and the proposed FS-MPCC (Method 3). In Method 2, the parameter K was defined as follows.

$$K = \frac{T_s}{L} = \frac{T_s}{\bar{L}} - \frac{\Delta\sigma_\alpha(k)}{\left[U_\alpha(k\text{-}1) - U_\alpha(k\text{-}2)\right]} \tag{28}$$

The comparison of the parameter K under $\bar{L} = 2\,L$ at 5 Nm load torque condition is displayed in Fig. 9. The results indicate that Method 3 can more precisely locate the value of the parameter K in different rotation speed from 400 r/min to 1200 r/min compared with Method 2. The experiment results also show that the obtained parameter K in Method 2 fluctuates greatly and the maximum amplitude of the obtained parameter K is 1.3 times larger than that in Method 3. The reference K means the value of the sampling period T_s divided by the nominal SPMSM inductance. It can be seen that the value of the obtained parameter K in Method 2 and Method 3 is close to the value of the reference K.

In this paper, the target motor speed is set through the load motor and the current performance between different methods is observed. The dynamic performance at 1000 r/min under $\bar{L} = 2\,L$ condition is shown in Fig. 10. Fig. 10(b), Fig. 10(e) and Fig. 10(h) show that Method 3 is the best performance either in fluctuation range or in tracking the reference current when the load torque steps from 2 Nm to 10 Nm and to 5 Nm. The performance of Method 1 is the worst. The performance from Method 2 shows similar performance in terms of tracking reference current but the torque ripple is worse than that of Method 3. The current on d axis is worst in Method 1. Defining f_{av} as the average switching frequency of the system, it can be seen that the f_{av} in Method 3 is lowest in the results. The dynamic performance at 800 r/min under $\overline{\Psi_m} = 1.5\ \Psi_m$ condition is shown Fig. 11. The quadrature axis current indicates that Method 3 is still the best. Fig. 12 shows the comparison at 800 r/min under $\bar{R} = 10\,R$ condition. The performance of Method 3 in tracking the reference current is much better than that of Method 1 and Method 2. From the results of f_{av}, it can be seen that the highest f_{av} is in Method 2.

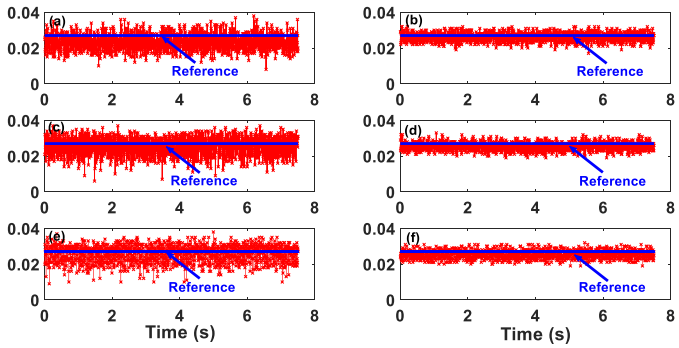

Fig. 9. Experimental results of the comparison of the parameter K under $\bar{L} = 2\,L$ at 5 Nm load torque condition. (a) K at 400 r/min in Method 2. (b) K at 400 r/min in Method 3. (c) K at 1000 r/min in Method 2. (d) K at 1000 r/min in Method 3. (e) K at 1200 r/min in Method 2. (f) K at 1200 r/min in Method 3.

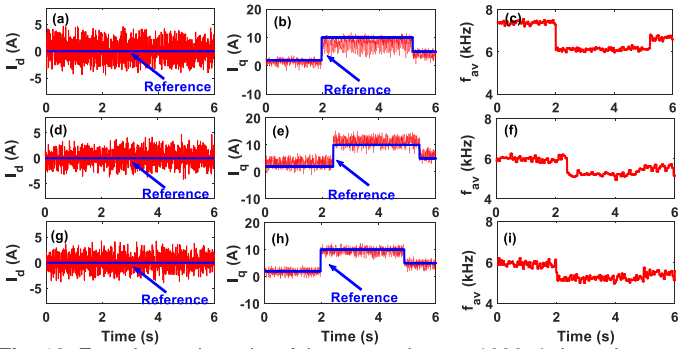

Fig. 10. Experimental results of the comparison at 1000 r/min under $\bar{L} = 2\,L$ condition. (a)–(c) Method 1. (d)–(f) Method 2. (g)–(i) Method 3.

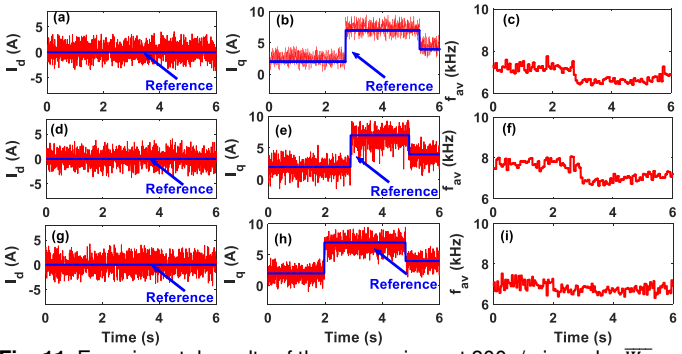

Fig. 11. Experimental results of the comparison at 800 r/min under $\overline{\Psi_m}$ = 1.5Ψ_m. (a)–(c) Method 1. (d)–(f) Method 2. (g)–(i) Method 3.

The current error between the reference and measure at different mismatch conditions is displayed in Fig. 13 and Fig. 14. The figures indicate that in different driving conditions, the lowest current error is Method 3, which means that Method 3 has the highest robustness compared with other methods.

The torque ripple assessment criterion refers in [30] and two mean absolute errors are presented as follows.

$$M_T = \frac{1}{N}\sum_{k=1}^{N}\left|e(k)\right| = \frac{1}{N}\sum_{k=1}^{N}\left|\left[T_e^{\,ref}(k) - T_e(k)\right]\right| \tag{29}$$

$$J_T = \sqrt{\frac{1}{N}\sum_{k=1}^{N}\left[T_e^{\,ref}(k) - T_e(k)\right]^2} \tag{30}$$

where N, $T_e(k)$ and $T_e^{\,ref}(k)$ stand for the total number of sampling points, measured electromagnetic torque and reference torque, respectively. A torque meter is utilized to measure the SPMSM electromagnetic torque. M_T and J_T are defined in Eq. (29) and Eq. (30), respectively. Fig. 15 and Fig.

16 show the torque ripple performance under different rotation speeds, which indicates that the proposed method shows minimum torque ripple.

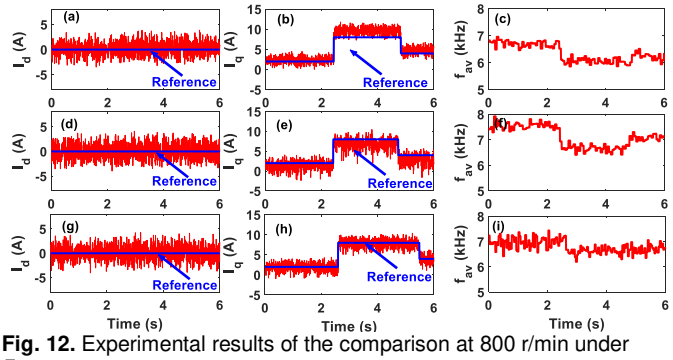

Fig. 12. Experimental results of the comparison at 800 r/min under $\bar{R} = 20\,R$ condition. (a)–(c) Method 1. (d)–(f) Method 2. (g)–(i) Method 3.

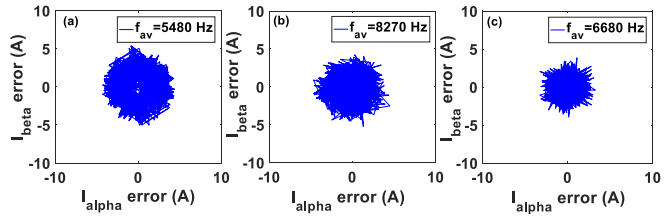

Fig. 13. Experimental results of currents error at 700 r/min under $\bar{L} = 0.5\,L$, $\overline{\Psi_m} = 1.5\,\Psi_m$ and $\bar{R} = 10\,R$ conditions. (a) Method 1. (b) Method 2. (c) Method 3.

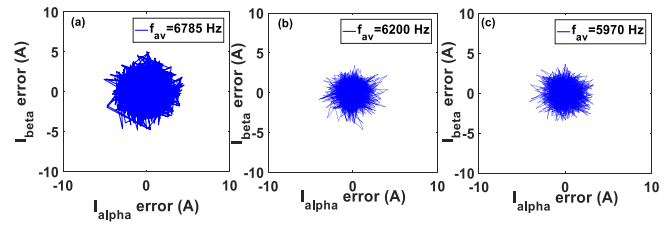

Fig. 14. Experimental results of currents error at 900 r/min under $\bar{L} = 2\,L$, $\overline{\Psi_m} = \Psi_m/3$ and $\bar{R} = 0.1\,R$ conditions. (a) Method 1. (b) Method 2. (c) Method 3.

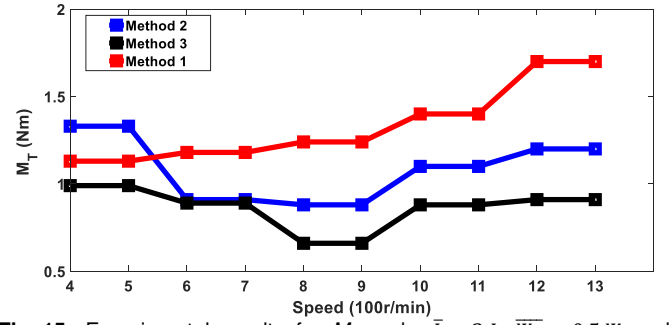

Fig. 15. Experimental results for M_T under $\bar{L} = 2\,L$, $\overline{\Psi_m} = 0.5\,\Psi_m$ and $\bar{R} = 10\,R$ conditions.

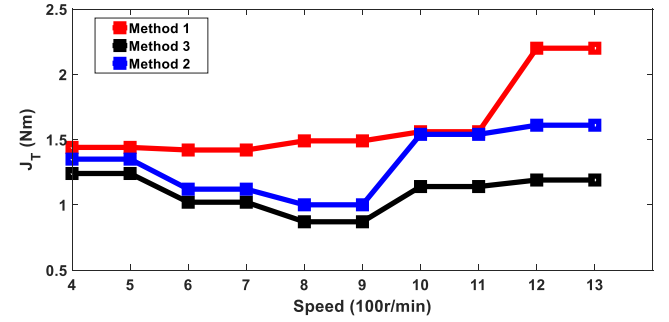

Fig. 16. Experimental results for J_T under $\bar{L} = 2\,L$, $\overline{\Psi_m} = 0.5\,\Psi_m$ and $\bar{R} = 10\,R$ conditions.

In addition, Fig. 17 shows the measured electromagnetic torque T_e and SPMSM speed under different mismatch conditions. The load torque is set to 5 Nm, and the speed considered is from 400 rpm to 800 rpm and then increase to 1200 rpm. From this figure, it can be seen that Method 3 has the best electromagnetic torque performance. To testify the response of the three methods, Fig. 18 shows the current on q axis under different mismatch conditions. The load torque is set from 1 Nm to 8 Nm. It can be seen that the response time T_r is almost 33 ms in the Method 1 while T_r in the Method 2 and Method 3 are almost 6 ms. This means that different mismatch condition can affect the response time. In addition, Method 3 has lower overshoot value of the current compared with Method 2. Fig. 19 shows that the current performance at 1500 r/min (rpm) under different mismatch conditions. The torque load is set to 6 Nm, and it can be seen that there is current offset in method 1 while the current ripple of Method 2 is larger than that in method 3. Therefore, at higher speed, such as 1500 r/min, method 3 can suppress the disturbances better than Method 2.

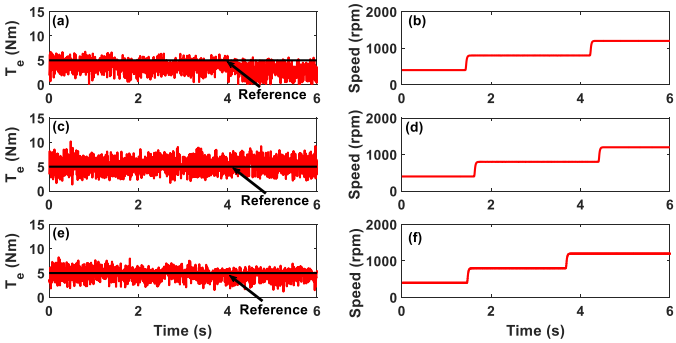

Fig. 17. Experimental results for the measured electromagnetic torque T_e and SPMSM speed under $\bar{L} = 2\,L$, $\overline{\Psi_m} = 0.5\,\Psi_m$ and $\bar{R} = 0.1\,R$ conditions. (a)–(b) Method 1. (c)–(d) Method 2. (e)–(f) Method 3.

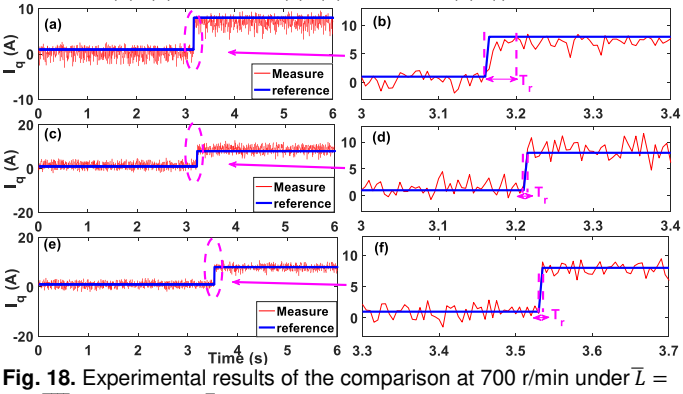

Fig. 18. Experimental results of the comparison at 700 r/min under $\bar{L} = 2\,L$, $\overline{\Psi_m} = 0.5\,\Psi_m$ and $\bar{R} = 5\,R$ conditions. (a)–(b) Method 1. (c)–(d) Method 2. (e)–(f) Method 3.

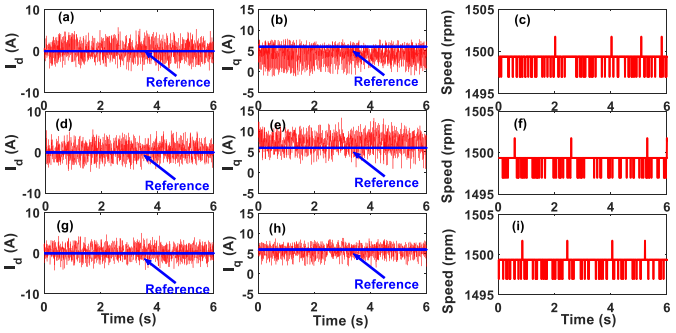

Fig. 19. Experimental results of the comparison at 1500 r/min under $\overline{L}$ = 2 L, $\overline{\Psi_{\mathrm{m}}}$ = 1.25 Ψ_{m} and $\bar{R}$ = 7 R conditions. (a)–(c) Method 1. (d)–(f) Method 2. (g)–(i) Method 3.

V. CONCLUSIONS

A novel current update mechanism is developed for FS-MPCC. The comparison of the proposed method and other methods is carried out systematically. Due to the state of the art of the current update mechanism, the predicted parameter K can be acquired more accurately. Experiment results indicate that when the system parameters are mismatched, the proposed method shows the best current performance. To illustrate this, various mismatched conditions are tested, and the torque ripple performance and tracking reference current performance are compared between new method and other methods. In addition, to verify the robustness of the proposed method, experiments under different rotation speeds and different load torques are carried out, and the experiment results indicate that the torque ripple performance of the proposed method is the best compared with other methods. Therefore, the proposed method can be experimentally applied in practical systems, which is significant towards FS-MPCC with parameter mismatch suppression for SPMSM drives.

REFERENCES

[1]. C. Yuan-Chih, C. Chien-Hua and Z. Zhong-Chuan, "Speed Control of the Surface-Mounted Permanent-Magnet Synchronous Motor Based on Takagi–Sugeno Fuzzy Models," IEEE Transactions on Power Electronics, vol.31, no.9, pp. 6504 - 6510, Sept. 2016.

[2]. O. Alejandro J. Piña and X. Longya, "Analytical Prediction of Torque Ripple in Surface-Mounted Permanent Magnet Motors Due to Manufacturing Variations," IEEE Transactions on Energy Conversion, vol.31, no.4, pp. 1634 - 1644, Dec. 2016.

[3]. J. Jin-Woo, L. Viet Quoc and D. Ton Duc, "Adaptive PID Speed Control Design for Permanent Magnet Synchronous Motor Drives," IEEE Transactions on Power Electronics, vol.30, no.2, pp. 900-908, Feb. 2015.

[4]. K. Samir, C. Patricio and V. RenÉ, "Model Predictive Control—A Simple and Powerful Method to Control Power Converters," IEEE Transactions on Industrial Electronics, vol.56, no.6, pp. 1826 - 1838, June. 2009.

[5]. A. Linder and R. Kennel, "Model predictive control for electrical drives," Proc. IEEE PESC, Recife, Brazil, pp. 1793–1799, June. 2005.

[6]. R. Jose, K. Marian P and E. Jose R, "State of the Art of Finite Control Set Model Predictive Control in Power Electronics," IEEE Transactions on Industrial Informatics, vol.9, no.2, pp. 1003 - 1016, May. 2013.

[7]. Y. Zhang and H. Yang, "Model Predictive Torque Control of Induction Motor Drives With Optimal Duty Cycle Control," IEEE Transactions on Power Electronics, vol.29, no.12, pp. 6593 - 6603, Dec. 2014.

[8]. Y. Zhang and H. Yang, "Two-Vector-Based Model Predictive Torque Control Without Weighting Factors for Induction Motor Drives," IEEE Transactions on Power Electronics,vol. 31, no. 2, pp. 1381-1390, Feb. 2016.

[9]. Y. Zhang and W. Xie, "Low Complexity Model Predictive Control—Single Vector-Based Approach," IEEE Transactions on Power Electronics, vol. 29, no. 10, pp. 5532 - 5541, Oct. 2014.

[10]. A. H. Jin and D. M. Lee, "A New Bumpless Rotor-Flux Position Estimation Scheme for Vector-Controlled Washing Machine," IEEE Transactions on Industrial Informatics, vol.12, no.2, pp. 466 - 473, April. 2016.

[11]. J. Rodas, F. Barrero, M. R. Arahal, C. Martín and R. Gregor, "Online Estimation of Rotor Variables in Predictive Current Controllers: A Case Study Using Five-Phase Induction Machines," IEEE Transactions on Industrial Electronics, vol.63, no.9, pp. 5348 - 5356, Sept. 2016.

[12]. X. Yuan, S. Zhang and C. Zhang, "Torque Ripple Suppression for Open-end Winding Permanent-Magnet Synchronous Machine Drives with Predictive Current Control" IEEE Transactions on Industrial Electronics, vol. 67, no. 3, pp. 1771 - 1781, March. 2020.

[13]. X. Zhang, L. Sun, K. Zhao and L. Sun, " Nonlinear Speed Control for PMSM System Using Sliding-Mode Control and Disturbance Compensation Techniques," IEEE Transactions on Power Electronics, vol.28, no.3, pp. 1358 - 1365, March. 2013.

[14]. X. Zhang, L. Zhang, and Y. Zhang, "A Model Predictive Current Control for PMSM Drives With Parameter Robustness Improvement." IEEE Transactions on Power Electronics, vol. 34, no. 2, pp. 1645 - 1657, Feb. 2019.

[15]. Z. Wang, A. Yu, X. Li, G. Zhang and C. Xia, "A Novel Current Predictive Control Based on Fuzzy Algorithm for PMSM," IEEE Journal of Emerging and Selected Topics in Power Electronics, vol. 7, no. 2, pp. 990 - 1001, June. 2019.

[16]. M. Yang, X. Lang, J. Long and D. Xu, "A Flux Immunity Robust Predictive Current Control With Incremental Model and Extended State Observer for PMSM Drive." IEEE Transactions on Power Electronics, vol. 32, no. 12, pp. 9267-9279, Dec. 2017.

[17]. J. Han, "From PID to Active Disturbance Rejection Control," IEEE Transactions on Industrial Electronics, vol.56, no.3, pp. 900 - 906, March. 2009.

[18]. C. Du, Z. Yin, Y. Zhang, X. Sun, J. Liu and Y. Zhong, "Decoupled current control of induction motors drives with internal model based on active disturbance rejection control strategy," 2016 19th International Conference on Electrical Machines and Systems (ICEMS), Nov. 2016.

[19]. X. Yuan, S. Zhang and C. Zhang, "Enhanced Robust Deadbeat Predictive Current Control for PMSM Drives," IEEE Access, vol. 7, pp. 148218 - 148230, Oct. 2019.

[20]. K. Lee and S. Kim, "Dynamic Performance Improvement of a Current Offset Error Compensator in Current Vector-Controlled SPMSM Drives," IEEE Transactions on Industrial Electronics, vol.66, no.9, pp. 6727 - 6736, Sept. 2019.

[21]. S. Li, and H. Gu, " Fuzzy Adaptive Internal Model Control Schemes for PMSM Speed-Regulation System," IEEE Transactions on Industrial Informatics, vol.8, no.4, pp. 767 - 779, Nov. 2012.

[22]. H. Nguyen and J. Jung, "Finite Control Set Model Predictive Control to Guarantee Stability and Robustness for Surface-Mounted PM Synchronous Motors," IEEE Transactions on Industrial Electronics, vol.65, no.11, pp. 8510 - 8519, Nov. 2018.

[23]. P. Wipasuramonton, Z.Q. Zhu and D. Howe, "Predictive current control with current-error correction for PM brushless AC drives." IEEE Transactions on Industrial applications, vol. 42, no. 4, pp. 1071-1079, Aug. 2006.

[24]. T. Türker, U. Buyukkeles, and A. F. Bakan, "A Robust Predictive Current Controller for PMSM Drives." IEEE Transactions on Industrial Electronics, vol. 63, no. 6, pp. 3906-3914, Jan. 2016.

[25]. H. Young, M. Perez and J. Rodriguez, "Analysis of Finite-Control-Set Model Predictive Current Control With Model Parameter Mismatch in a Three-Phase Inverter." IEEE Transactions on Industrial Electronics, vol. 63, no. 5, pp. 3100 - 3107, May. 2016.

[26]. C. K. Lin, T. H. Liu, J. T. Yu, L. C. Fu and C. F. Hsiao, "Model-Free Predictive Current Control for Interior Permanent-Magnet Synchronous Motor Drives Based on Current Difference Detection Technique," IEEE Transactions on Industrial Electronics, vol. 61, no. 2, pp. 667-681, Feb. 2014.

[27]. C. Lin, J. Yu, Y. Lai and H. Yu, "Improved Model-Free Predictive Current Control for Synchronous Reluctance Motor Drives," IEEE Transactions on Industrial Electronics, vol. 63, no. 6, pp. 3942-3953, June 2016.

[28]. M. Siami, D. A. Khaburi, A. Abbaszadeh and J. Rodríguez, "Robustness Improvement of Predictive Current Control Using Prediction Error Correction for Permanent-Magnet Synchronous Machines," IEEE Transactions on Industrial Electronics, vol. 63, no. 6, pp. 3458-3466, June. 2016.

[29]. M. Siami, D. A. Khaburi and J. Rodriguez, "Torque Ripple Reduction of Predictive Torque Control for PMSM Drives with Parameter Mismatch," IEEE Transactions on Power Electronics, vol. 32, no. 9, pp. 7160 - 7168, Sep. 2017.

[30]. X. Yuan, S. Zhang and C. Zhang, "Improved Model Predictive Current Control for SPMSM Drives with Parameter Mismatch," IEEE Transactions on Industrial Electronics, vol. 67, no. 2, pp. 852 - 862, Feb. 2020.

[31]. I. Jeong, B. Hyon and K. Nam, "Dynamic Modeling and Control for SPMSMs With Internal Turn Short Fault," IEEE Transactions on Power Electronics, vol. 28, no. 7, pp. 3495 - 3508, Feb. 2013.

[32]. Y. Wang, J. Zhu, S. Wang, Y. Guo and W. Xu, "Nonlinear Magnetic Model of Surface Mounted PM Machines Incorporating Saturation

Saliency," IEEE Transactions on Magnetics, vol. 45, no. 10, pp. 4684 - 4687, Oct. 2009.

[33]. P. Cortes, J. Rodriguez, C. Silva and A. Flores, "Delay Compensation in Model Predictive Current Control of a Three-Phase Inverter," IEEE Transactions on Industrial Electronics, vol. 59, no. 2, pp. 1323-1325, Feb. 2012.

Xin Yuan (S'19) was born in Heilongjiang, China, in 1990. He received the B.Eng. and M.Sc. degrees in electrical engineering, in 2013 and 2016, respectively.

He is currently a Ph.D. candidate at National Engineering Laboratory for Electric Vehicles and School of Mechanical Engineering, Beijing Institute of Technology. He is a research associate in PEMC group, University of Nottingham since Jan. 2019. His research interests include synchronous motor drives, power converters, multi-phase motor drives and fault-tolerant strategy of motor.

Shuo Zhang received the B.Eng. degree from North China Institute of Aerospace Engineering, Hebei, China, in 2011, and he received the Ph.D. degree in vehicle engineering from the Beijing Institute of Technology, Beijing, China, in 2017.

He is currently an assistant professor at National Engineering Laboratory for Electric Vehicles and School of Mechanical Engineering, Beijing Institute of Technology. His research interests include the modeling and control for the permanent magnet synchronous motor, multi-motor driving system and hybrid power system.

Chengning Zhang received the M.E. degree in control theory and control engineering and the Ph.D. degree in vehicle engineering from the Beijing Institute of Technology, Beijing, China, in 1989 and 2001, respectively.

He is currently a Professor and the Vice Director of the National Engineering Laboratory for Electric Vehicles, Beijing Institute of Technology. His research interests include electric vehicles, vehicular electric motor drive systems, battery management systems, and chargers.

Alessandro Galassini (S'13-M'17) received the Master's degree in Mechatronic Engineering in 2012 from the University of Modena and Reggio Emilia, Reggio Emilia, Italy. In 2017, he received the Ph.D. degree in power sharing for multi-three-phase electrical machines from the University of Nottingham, Nottingham, U.K. Currently, he is a Researcher with the Power Electronics, Machines and Control Group group, The University of Nottingham, Nottingham, U.K., and his research area is focused on control of electrical drives for future transportation systems.

Giampaolo Buticchi (S'10-M'13-SM'17) received the Master degree in Electronic Engineering in 2009 and the Ph.D degree in Information Technologies in 2013 from the University of Parma, Italy. In 2012 he was visiting researcher at The University of Nottingham, UK. Between 2014 and 2017, he was a post-doctoral researcher and Von Humboldt Post-doctoral Fellow at the University of Kiel, Germany.

He is now Associate Professor in Electrical Engineering at The University of Nottingham Ningbo China and the Head of Power Electronics of the Nottingham Electrification Center. His research focuses on power electronics for renewable energy systems, smart transformer fed micro-grids and dc grids for the More Electric Aircraft. He is author/co-author of more than 190 scientific papers and an Associate Editor of the IEEE Transactions on Industrial Electronics, of the IEEE Open Journal of the Industrial Electronics Society and of the IEEE Transactions on Transportation Electrification.

He is the Chair of the IEEE Industrial Electronics Society Technical Committee on Renewable Energy Systems.

Michele Degano (M'15) received the Laurea degree in electrical engineering from the University of Trieste, Trieste, Italy, in 2011, and the Ph.D. degree in industrial engineering from the University of Padova, Padova, Italy in 2015. In 2015, he joined the Power Electronics, Machines and Control Group, The University of Nottingham, Nottingham, U.K., as a Research Fellow, where he is currently an Assistant Professor teaching advanced courses on electrical machines. His main research interests include design and optimization of permanent-magnet machines, reluctance and permanent-magnet-assisted synchronous reluctance motors through genetic optimization techniques, for automotive and aerospace applications.